AIAA 82-4175

Aeroelastic Stability of Space Shuttle Protuberances

L.E. Ericsson* and J.P. Reding†
Lockheed Missiles and Space Company, Inc., Sunnyvale, Calif.

The cable trays of rectangular cross section that carry the cables over the hydrogen-oxygen (HO) tank surface on the Space Shuttle launch vehicle encounter high cross-flow velocities, induced by the bow shock from the solid rocket booster (SRB) at transonic and supersonic speeds. A few cable tray sections experience 90-deg cross-flow and several sections are subject to cross flow between 60 and 90 deg. An analysis of the aeroelastic characteristics of these cable tray sections indicated that the structural integrity of the cable trays could not be ensured. Consequently, it was decided to use an aerodynamic fix, consisting of a 20-deg flow ramp, on the first Space Shuttle launch vehicle, which flew successfully April 12, 1981.

Nomenclature

b = span
c = two-dimensional chord length
d = body diameter
d^l = drag, coefficient $c_d = d^l/(\rho V^2/2)c$
f = frequency
H = altitude
h = cross-sectional height of cable tray
l = sectional lift, coefficient $c_l = l/(\rho V^2/2)c$
M = Mach number
M_p = pitching moment, coefficient $C_m = M_p/(\rho_\infty U_\infty^2/2)Sd$
$\tilde{m}$ = generalized mass
m_p = sectional pitching moment, coefficient $c_m = m_p/(\rho V^2/2)c^2$
N = normal force, coefficient $C_N = N/(\rho_\infty U_\infty^2/2)S$
n = sectional normal force, coefficient $c_n = n/(\rho V^2/2)c$
p = static pressure, coefficient $C_p = (p-p_\infty)/(\rho V^2/2)$
$P(t)$ = generalized force
q = pitch rate
$q(t)$ = normalized coordinate
Re, Re_x = Reynolds number, $Re = Vc/\nu_\infty$, $Re_x = Vx/\nu_\infty$
r_I = radius of torsional inertia
S = reference area $= \pi d^2/4$
T = torsional moment
t = time
U = axial velocity
V = cross-flow velocity
$\bar{V}$ = reduced velocity $= V/fh$
x = horizontal body coordinate, axial in three-dimensional and chordwise in two-dimensional flow
y = spanwise coordinate
z = vertical coordinate, Fig. 6
α = angle of attack
Δ = increment and amplitude
Δt = time lag
$\zeta_a + \zeta_s$ = aerodynamic damping, fraction of critical
ζ_0 = structural damping, fraction of critical
η = dimensionless y coordinate $= y/b$
θ = perturbation in pitch and torsion
κ = dimensionless radius of torsional inertia $= 2r_I/c$
ν = kinematic viscosity of air
ξ = dimensionless x coordinate $= x/c$
ξ_{sp} = effect of separation point movement, Eq. (23)
ξ_w = Karman-Sears wake lag parameter, Eq. (29)
ρ = air density
$\tilde{\rho}_{CT}$ = effective density of cable tray
ϕ = normalized modal deflection
ω = angular frequency $= 2\pi f$
$\bar{\omega}$ = reduced frequency $= \omega c/V$ or $\omega c/U$

Subscripts and Superscripts

a = attached flow
CT = cable tray
E = external
$(\ )_i$ = controlling flow separation
$(\ )^i$ = separation induced; e.g., $\Delta^i C_N$ = separation-induced normal force
max = maximum
OC = oscillation center and moment reference axis
s = separated flow
sp = separation point
V = V component
0 = initial or time-average value
$1,2,3\ldots$ = numbering subscripts
∞ = freestream conditions
$(\ )'$ = sectional force referenced to frontal area; e.g., $c_n' = n/(\rho V^2/2)h$

Derivative Symbols

$$c_{mq} = \frac{\partial c_m}{\partial (cq/V)}$$

$$c_{m\alpha} = \frac{\partial c_m}{\partial \alpha}$$

$$c_{m\dot{\alpha}} = \frac{\partial c_m}{\partial (c\dot{\alpha}/V)}$$

$$c_{m\theta} = c_{mq} + c_{m\dot{\alpha}}$$

$$\dot{\alpha} = \frac{\partial \alpha}{\partial t} \cdot \ddot{q} = \frac{\partial^2 q}{\partial t^2}$$

Introduction

OF the various cable trays present on the main Space Shuttle booster, the hydrogen-oxygen (HO) tank (Fig. 1), the LO_2 cable tray was of special concern because of its low margin of safety. Examination of the LO_2 tank flowfield revealed that the interference from the nose cone of the adjacent solid rocket booster (SRB) subjects the LO_2 cable tray to large cross-flow angles, up to 90 deg, at transonic and low supersonic speeds (Figs. 2 and 3). The rectangular cross section of the cable tray (Fig. 4) causes its aerodynamics to be dominated by separated flow. The separation-induced loads,

Received Sept. 14, 1981; revision received Jan. 27, 1982.

*Senior Consulting Engineer. Associate Fellow AIAA.
†Staff Engineer. Associate Fellow AIAA.

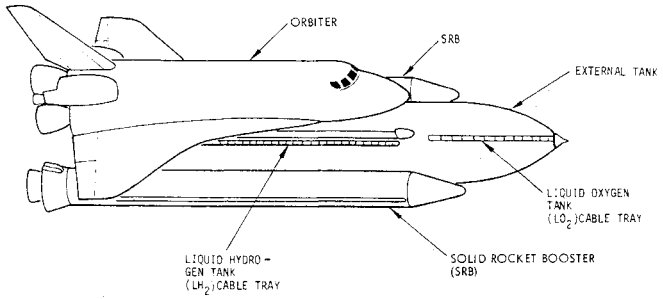

Fig. 1 Space Shuttle launch configuration.

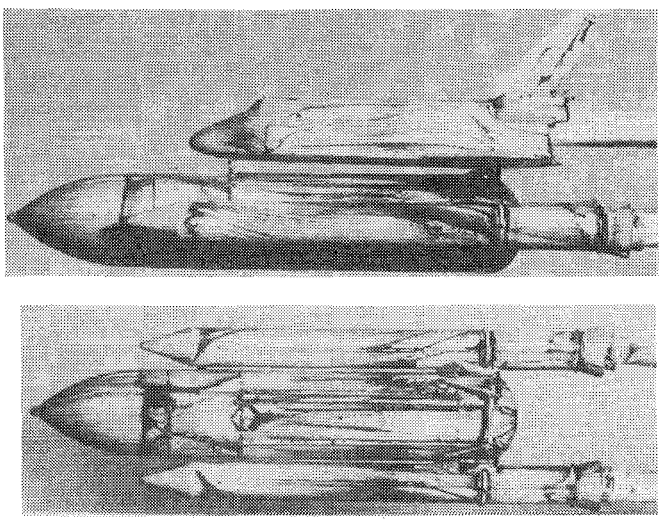

Fig. 2 Oil flow photographs of HO and SRB tanks at $\alpha = 0.26$ deg and $M = 1.1$.

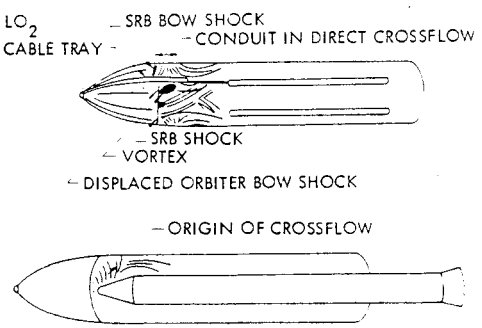

Fig. 3 Interpretative flow sketches of oil flow photographs.

which are statically stabilizing[1] (Fig. 5), will be dynamically destabilizing owing to the time lag associated with the aerodynamic loads induced by separated flow.[2-6] To determine whether or not these adverse, unsteady aerodynamics can cause aeroelastic instability of sufficient magnitude to endanger the structural integrity of the LO_2 cable tray is the purpose of the present analysis.

Analysis

The dynamics of the cable tray are analyzed for oscillations in torsion, the critical degree of freedom.[7] The equation of motion can be written in the following form using standard notations:

$$\tilde{m}[\ddot{q}(t) + 2\zeta_0 \omega \dot{q}(t) + \omega^2 q(t)] = P(t) \tag{1}$$

The generalized force $P(t)$ is given by the virtual work‡ done by the aerodynamic forces and moments.

‡If W is the work done, $P = \partial W / \partial q$.

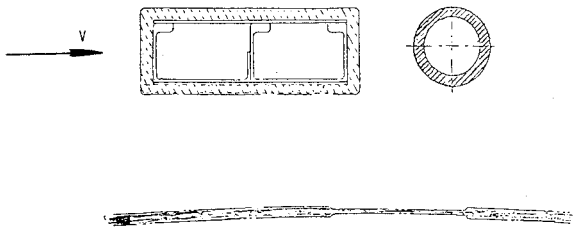

Fig. 4 Initial LO_2 tank cable tray configuration.

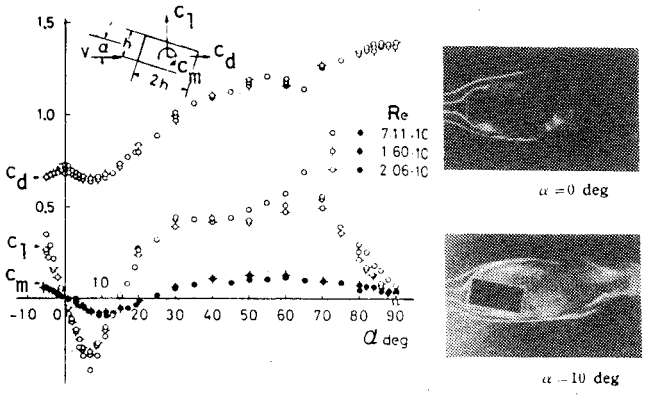

Fig. 5 Aerodynamic characteristics of a rectangular prism.[1]

For the torsional degrees of freedom $P(t)$ becomes

$$P(t) = \int \frac{dT}{dy} \phi(y)\, dy \tag{2}$$

where dT/dy is the torsional pitching moment per unit span and $\phi(y)$ is the normalized torsion mode.

There are three different types of generalized force,

$$P(t) = P_s(t) + P_a(t) + P_f(t) \tag{3}$$

where $P_s(t)$ is the generalized force in separated flow, $P_a(t)$ the generalized force in attached flow, and $P_f(t)$ the generalized force independent of body motion, e.g., due to buffeting or vortex wakes.

While $P_a(t)$ and $P_f(t)$ usually can be defined by well-established methods, $P_s(t)$ can often not be defined without a special analysis tailored to the problem at hand. Thus the main effort is devoted to the description of $P_s(t)$.

Figure 6 shows the cable tray in cross flow of velocity V. For small perturbations the sectional aerodynamic force and moment induced by separated flow can be expressed in derivative form as follows§:

$$\frac{dT_s}{dy} = M_s = \frac{\rho V^2}{2} c^2 \left[\Delta^i c_{m_\theta} \left(\theta + \frac{\dot{z}}{V} \right) + \Delta^i c_{m_{\dot\theta}} \frac{c\dot\theta}{V} \right] \tag{4}$$

The corresponding expression for the attached flow derivatives is

$$\frac{dT_a}{dy} = M_a = \frac{\rho V^2}{2} c^2 \left[c_{m_\theta} \left(\theta + \frac{\dot{z}}{V} \right) + c_{m_{\dot\theta}} \frac{c\dot\theta}{V} \right] \tag{5}$$

§The aerodynamic acceleration derivatives are assumed negligible compared to the structural counterparts. All aerodynamic ground-interference-type terms, $c_m(z)$, associated with the height z of the tray above the surface of the ET are also assumed to be negligible. This is probably a good assumption for the initial cable tray cross section (Fig. 4).

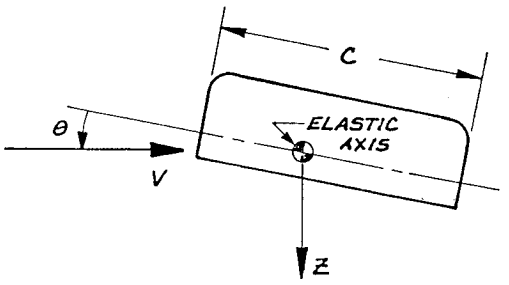

Fig. 6 Definition of cable tray coordinates.

Equations (1-5) give the following results¶:

$$\ddot{q}(t)+2\omega(\zeta_0+\zeta_a+\zeta_s)\dot{q}(t)+\omega^2 q(t)=P_f(t)/\tilde{m} \tag{6}$$

With $\eta=y/b$, where b is the spanwise distance between cable tray supports, $\zeta_a+\zeta_s$ can be written as follows for constant cross-flow velocity:

$$\zeta_a+\zeta_s=-\frac{\rho Vc^3 b}{4\omega\tilde{m}}\left(c_{m_{\dot\theta}}+\Delta^i c_{m_{\dot\theta}}\right)\int_0^1 \phi^2(\eta)\,\mathrm{d}\eta \tag{7}$$

For the cable tray with constant cross section, $c\times h$, the generalized mass can be expressed in the following form:

$$\tilde{m}=\tilde{\rho}_{\mathrm{CT}} r_I^2 hcb\int_0^1 \phi^2(\eta)\,\mathrm{d}\eta \tag{8}$$

$\tilde{\rho}_{\mathrm{CT}}$ is the effective average density of the cable tray and r_I is the cross-sectional radius of inertia in torsion. Substituting $r_I=\kappa c/2$ and $\phi=\phi_0+(1-\phi_0)\sin(n\pi\eta)$** in Eq. (8) gives for the nth mode,

$$\kappa^2\tilde{\rho}_{\mathrm{CT}}=4\tilde{m}/hc^3 b\left\{\frac{1-2\phi_0+3\phi_0^2}{2}-\frac{2\phi_0(1-\phi_0)}{n\pi}\right.$$

$$\left.\times\left[(-1)^n-1\right]\right\} \tag{9a}$$

For fixed end points, $\phi_0=0$, Eq. (9a) reduces to

$$\kappa^2\tilde{\rho}_{\mathrm{CT}}=8\tilde{m}/hc^3 b \tag{9b}$$

Combining Eqs. (7) and (8), the aerodynamic damping can be defined as follows:

$$\zeta_a+\zeta_s=-\frac{1}{2\pi\kappa^2}\frac{\rho}{\tilde{\rho}_{\mathrm{CT}}}\bar{V}\left(c_{m_{\dot\theta}}+\Delta^i c_{m_{\dot\theta}}\right) \tag{10}$$

Aerodynamic Damping

The minimum value of the structural damping for aeroelastic stability in torsion, determined by Eqs. (6) and (10), is

$$\zeta_0>\frac{1}{2\pi\kappa^2}\frac{\rho}{\tilde{\rho}_{\mathrm{CT}}}\bar{V}\left(c_{m_{\dot\theta}}+\Delta^i c_{m_{\dot\theta}}\right) \tag{11}$$

Studying the pressure distribution on rectangular cross sections[8,9] the load distribution shown in Fig. 7 was obtained (the "primed" coefficient is based on the frontal area rather than on the horizontal area). The effect of Mach number was assumed to be similar to that measured on a flat-faced cylinder[10] (Fig. 8), resulting in the lumped load characteristics

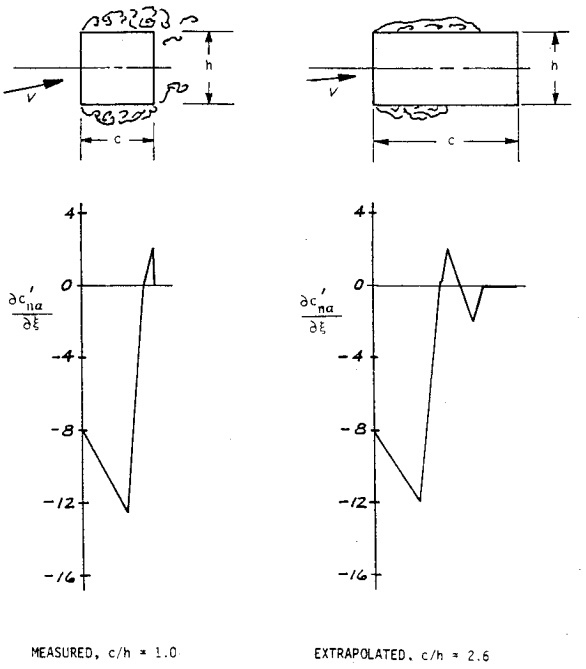

Fig. 7 Normal force derivative distribution on rectangular prisms in incompressible flow at $\alpha=0$.

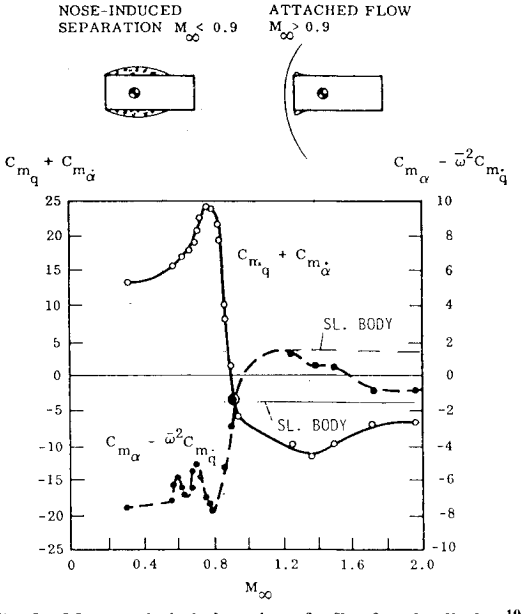

Fig. 8 Measured pitch damping of a flat-faced cylinder.[10]

shown in Fig. 9. To be conservative the peak value is used until $M=M_a=0.9$.

Thus, having obtained an estimate of the static aerodynamics, the next step is to obtain the dynamic characteristics by determining the phase relationship for the lumped load relative to the body motion. This has been done for blunt-nosed cylinder-flare bodies with good success,[11] and one would expect that the lumped load phase relationships established for the cylinder-flare body[11] could be modified and applied to the cylinder-alone body in Fig. 8. For the negative nose load component one obtains the situation sketched in Fig. 10. The phasing is caused by the effective†† time lag Δt. The figure shows how in the static case the separation-induced force $\Delta^i C_N(t)$ at $\alpha>0$ is stabilizing,

¶Neglecting ground interference from the ET surface.

**This is shown in Ref. 7 to be a good representation of the mode shape.

††Even effects that are not due to convective time lag can be represented mathematically by an effective time lag.

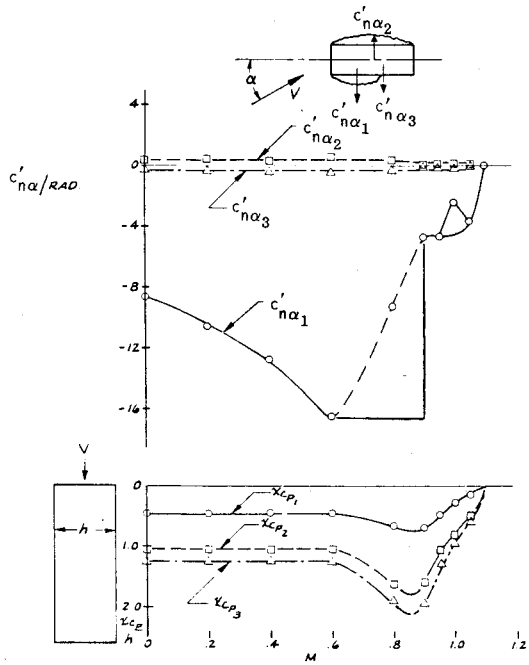

Fig. 9 Estimated lumped load derivatives for the cable tray.

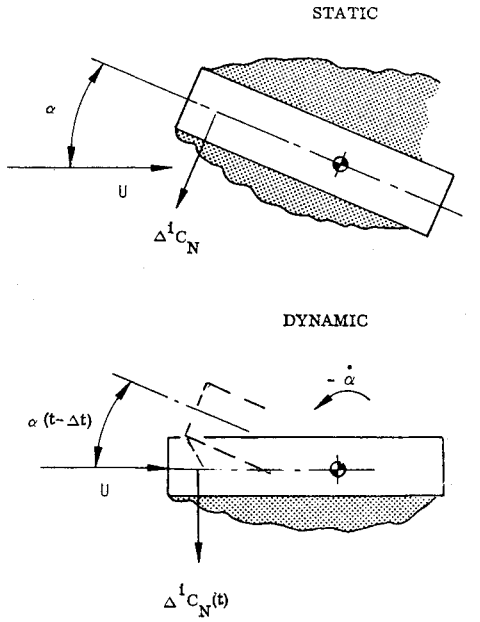

Fig. 10 Sketch of effective time lag effects.

whereas in the dynamic case the residual force, $\Delta^i C_N(t)$ at $\alpha = 0$ and time t, is generated by the flow separation created at the earlier time $t-\Delta t$, when $\alpha(t-\Delta t) > 0$, thus generating a residual force that drives the motion and hence is dynamically destabilizing.

With $\alpha(t) = \alpha_0 + \theta(t)$, one obtains for $\Delta^i C_{N_s}(t)$,

$$\Delta^i C_{N_s}(t) = \Delta^i C_{N\alpha_s} \alpha_i(t)$$
$$\alpha_i(t) = \alpha_0 + \theta(t-\Delta t) \tag{12}$$

For harmonic oscillations, $\theta = \Delta\theta \sin(\omega t)$, $\theta(t-\Delta t)$ can be written

$$\theta(t-\Delta t) = \Delta\theta \sin\omega t \cos\omega\Delta t - \Delta\theta \cos\omega t \sin\omega\Delta t \tag{13}$$

That is,

$$\theta(t-\Delta t) = \theta\cos\omega\Delta t - (\dot{\theta}/\omega)\sin\omega\Delta t \tag{14}$$

With $\Delta t = c\Delta\tau/U$, i.e., using the dimensionless time lag $\Delta\tau$, which denotes the amount of reference lengths ($c=d$) that the vehicle travels during the physical time lag Δt, one obtains the following expression for Eq. (14):

$$\theta(t-\Delta t) = \theta\cos(\bar{\omega}\Delta\tau) - \frac{c\dot{\theta}}{U}\frac{\sin(\bar{\omega}\Delta\tau)}{\bar{\omega}} \tag{15}$$

Thus the separation-induced pitch damping derivative component $\Delta^i C_{N_{\dot{\theta}_s}} = \partial \Delta^i C_{N_s} / \partial(c\dot{\theta}/U)$ is defined by Eqs. (12) and (15) as follows:

$$\Delta^i C_{N_{\dot{\theta}_s}} = -\frac{\sin(\bar{\omega}\Delta\tau)}{\bar{\omega}} \Delta^i C_{N_{\alpha_s}} \tag{16}$$

For slow oscillations, $\bar{\omega}\Delta\tau \le 0.2$, Eq. (16) simplifies to

$$\Delta^i C_{N_{\dot{\theta}_s}} \sim -\Delta\tau \Delta^i C_{N_{\alpha_s}} \tag{17}$$

Thus‡‡

$$\Delta\tau = -\Delta^i C_{N_{\dot{\theta}_s}} / \Delta^i C_{N_{\alpha_s}} = -\Delta^i C_{m_{\dot{\theta}_s}} / \Delta^i C_{m_{\alpha_s}} \tag{18}$$

The separation-induced effects, $\Delta^i C_{N_{\alpha_s}}$ and $\Delta^i C_{m_{\alpha_s}}$, are the differences between the measured values at $M < M_a$ and the "supersonic" levels at $M > M_a$, where $M_a < 1.0$. Figure 8 shows the supersonic levels at $M \ge M_a$ to approach the slender body values. With these as the attached flow reference levels the figure gives

$$\Delta\tau = -\Delta^i C_{m_{\dot{\theta}_s}} / \Delta^i C_{m_{\alpha_s}}$$
$$1.9 \le \Delta\tau \le 3.1 \tag{19}$$

The low value for $\Delta\tau$ is obtained at $M_\infty = 0.4$ and the high limit at $M_\infty = 0.8$.

From the dynamic stall analysis in Refs. 12 and 13 one obtains the following value for the dimensionless time lag when nose stall has occurred. This would be the case applicable to the cable tray, which has nose stall already at $\alpha = 0$ at $M < M_a$,

$$\Delta\tau = \xi_w + \xi_{sp} \tag{20}$$

where $\xi_w = 1.5$.

The value for ξ_{sp} is zero when the separation point is fixed,[12,13] as in the case of a sharp-edged rectangular cross section. When the leading edge is rounded, as in the case of the LO_2 cable tray (Fig. 4), ξ_{sp} takes the following values:

$$\xi_{sp} = 0.75 \quad \text{turbulent stall}$$
$$= 3.0 \quad \text{laminar stall} \tag{21}$$

Thus one obtains

$$2.25 \le \Delta\tau \le 4.5 \tag{22}$$

The rather good agreement between the three- and two-dimensional time lag values, Eqs. (19) and (22), respectively, is reassuring. Combining Eqs. (18) and (22) gives

$$-2.25 \le \Delta^i c_{m_{\dot{\theta}_s}} / \Delta^i c_{m_{\alpha_s}} \le -4.5 \tag{23}$$

‡‡The lever arm to the separation-induced force is the same in the static as in the dynamic case, and $\Delta^i(C_{m_\alpha} - \bar{\omega}^2 C_{m_{\dot{q}}}) \approx \Delta^i C_{m_\alpha}$, as $\bar{\omega}^2 \ll 1$.

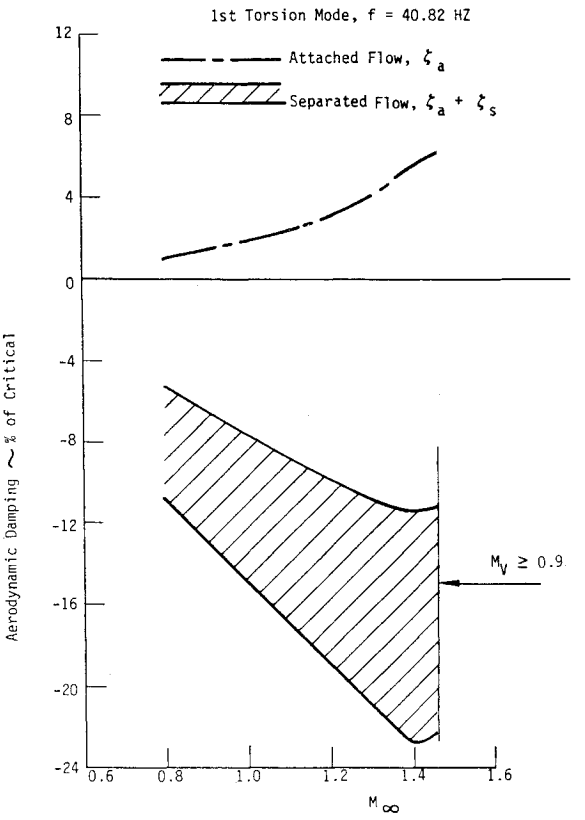

Fig. 11 Computed aerodynamic damping of cable tray torsional oscillations in subsonic cross flow.

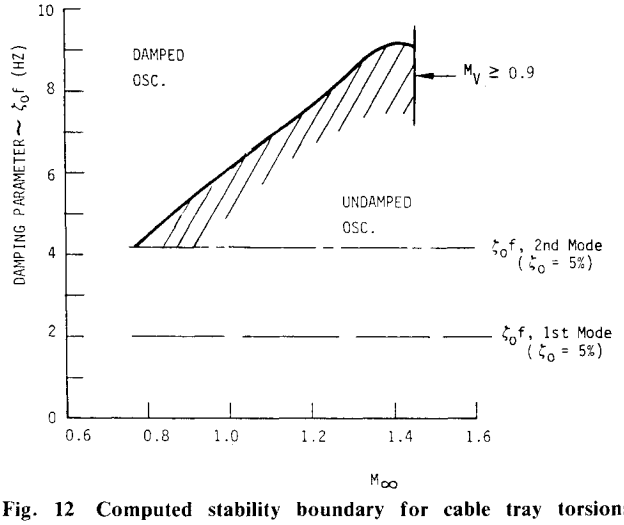

Fig. 12 Computed stability boundary for cable tray torsional oscillations.

From Fig. 9 one obtains for $0 \leq M < M_a$ the following moment around midchord

$$\Delta^i c_{m_{\alpha_s}} \approx 0.33 c_{n_{\alpha_l}} \tag{24}$$

Assuming that the attached flow-type derivative, $c_{m_{\dot{\theta}}}$, is of negligible magnitude in the nose-induced separated flow region existing at $0 < M < M_a$, one obtains from Eqs. (23) and (24) the following estimate of the aerodynamic damping derivative:

$$0.75 \leq (c_{m_{\dot{\theta}}} + \Delta^i c_{m_{\dot{\theta}}}) / -c_{n_{\alpha_l}} \leq 1.5 \tag{25}$$

where $c_{n_{\alpha_l}} = c'_{n_{\alpha_l}} / 2.6$ for the LO_2 cable tray, with $c'_{n_{\alpha_l}}$ given by the solid line in Fig. 9.

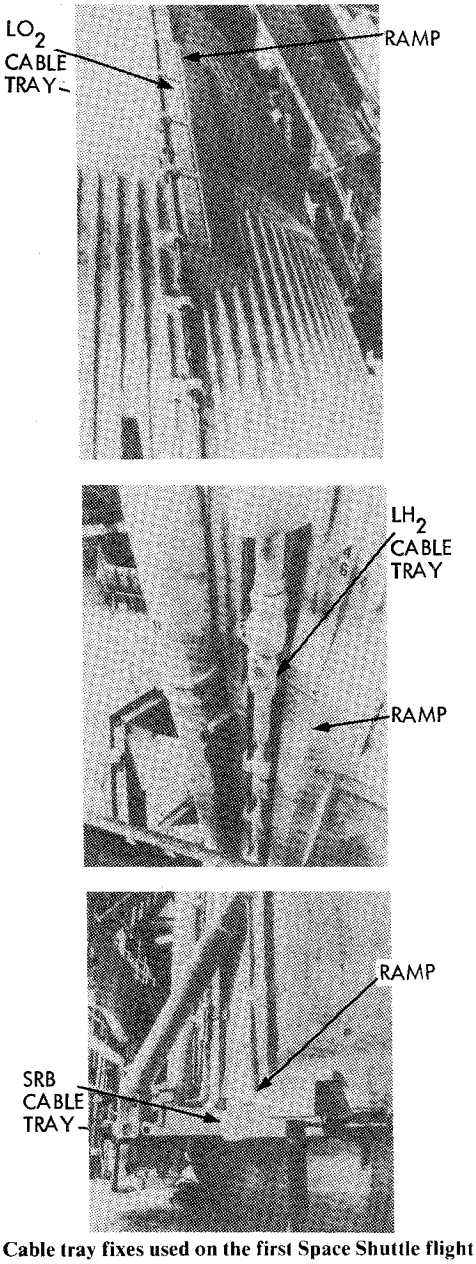

Fig. 13 Cable tray fixes used on the first Space Shuttle flight vehicle.

Using Eqs. (9), (10), (24), and (25) together with the measured local environment[7] gives the aerodynamic damping for the first torsion mode ($f = 40.82$ Hz, Ref. 7) shown in Fig. 11. The upper and lower boundaries of $\zeta_a + \zeta_s$ are essentially due to Eq. (25). The attached flow damping, ζ_a, in Fig. 11 was obtained as follows, using the analytic tools developed in Refs. 12-15:

$$c_{m_{\dot{\theta}_a}} = c_{n_\alpha} [\xi_w (0.25 - \xi_{OC}) + 0.25(\xi_{OC} - 0.75)] \tag{26}$$

where

$$\begin{aligned} \xi_w &= 1.5 \qquad \bar{\omega} \leq 0.16 \\ &= 0.245/\bar{\omega} \qquad \bar{\omega} > 0.16 \end{aligned} \tag{27}$$

With the value $c_{n_\alpha} \approx 5.5$ for the cable tray, $\xi_{OC} = 0.5$, and $\bar{\omega} \geq 0.16$, Eqs. (26) and (27) give

$$\begin{aligned} c_{m_{\dot{\theta}_a}} &\approx -0.345(1 + \bar{\omega}^{-1}) \\ &= -0.345\left(1 + \frac{\bar{V}}{2\pi} \frac{h}{c}\right) \end{aligned} \tag{28}$$

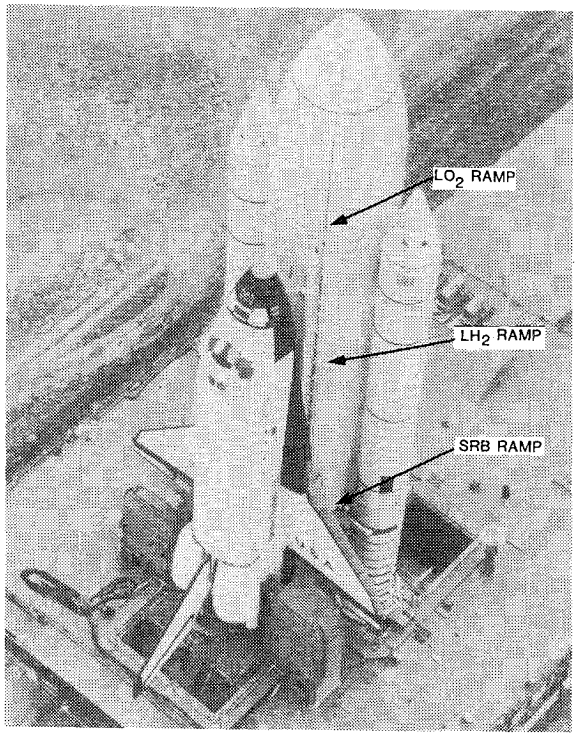

Fig. 14 Aerodynamic fixes on first Space Shuttle flight vehicle.

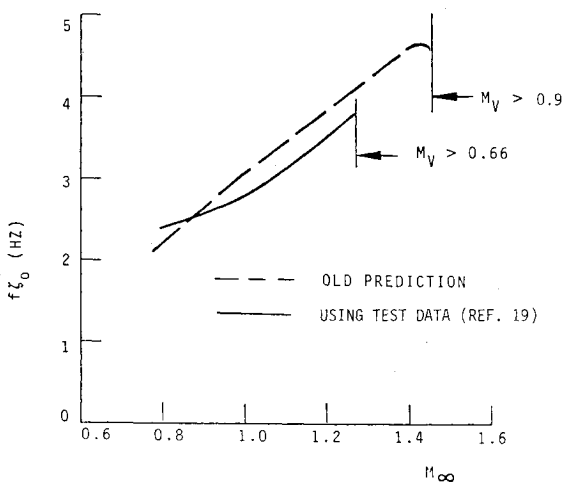

Fig. 15 Comparison between old and new stability boundaries.

Thus, for the cable tray with $c/h = 2.6$,

$$c_{m_{\dot\theta_a}} = -0.345(1 + \bar{V}/16.3) \tag{29}$$

Figure 11 shows that 5% structural damping, $\zeta_0 = 5\%$, is not sufficient to insure aeroelastic stability for torsional oscillations in the lowest mode,[7] $f = 40.82$ Hz.

The requirement for damped oscillations expressed in Eq. (11) can be written

$$\frac{\zeta_0 fh}{V} > \frac{I}{2\pi\kappa^2}\,\frac{\rho}{\bar{\rho}_{CT}}\,(c_{m_{\dot\theta}} + \Delta^i c_{m_{\dot\theta}}) \tag{30}$$

The upper, most conservative, stability boundary defined by Eq. (30) is shown in Fig. 12, revealing that not only the first, but also the second, torsional mode[7] ($f = 83.45$ Hz) will be aeroelastically unstable for $\zeta_0 = 5\%$.

The above analysis is only valid for $M_V < M_a$, where $M_a = 0.9$ has been assumed. At $M_V > 0.9$ the aerodynamics become discontinuous in character and one has to perform a nonlinear analysis, as is described in Refs. 7 and 16.

The results of the above analysis indicated that the structural integrity of the LO_2 cable tray could not be assured with the existing design. The same was also true for the two aft SRB cable trays, which were directly exposed to the full axial flow over the HO tank. It was, therefore, decided that on the first Space Shuttle flight vehicle 20-deg flow ramps would be applied as upstream wind shields for the LO_2 and SRB cable trays, and also for some sections of the LH_2 cable trays (Fig. 13). The ramps for the different cable trays are visible in the pictures of the roll out of the first flight vehicle[17,18] (Fig. 14).

The analysis presented here was by necessity very conservative, as neither static nor dynamic test results were available for the actual cable tray cross section. However, the final analysis,[7] in which such experimental data was used, led to the same conclusion in regard to the need for aerodynamic fixes. The dynamic test[19] also verified the soundness of the time lag concept used in the initial analysis, as is illustrated by the comparison in Fig. 15 between the "old" prediction (Fig. 12) and the aeroelastic stability boundary obtained using the measured[19] aerodynamic characteristics for the original LO_2 cable tray cross section. The agreement is remarkably good. The main difference is the change of the limiting Mach number for continuous subsonic aerodynamic characteristics from the assumed value $M_a = 0.9$ to 0.66.

Conclusions

An aeroelastic analysis of the Space Shuttle cable trays shows that cable tray sections experiencing 60-90-deg cross flow are aeroelastically unstable for torsional oscillations in the complete Mach number range investigated. Thus flow-ramp-type aerodynamic fixes were installed on the first Space Shuttle launch vehicle to assure the structural integrity of the cable trays.

Acknowledgments

The paper is based upon results obtained in work done under contract to Martin-Marietta Corporation, Michoud Operations, New Orleans, La., with D.B. Schwartz as the contract coordinator. The possibility of an aeroelastic problem for the Space Shuttle cable trays was first brought to the authors' attention by P.S. Woods, Martin Marietta Corporation, Denver Division, Denver, Colo.

References

[1] Nakamura, Y. and Mizota, T., "Aerodynamic Characteristics and Flow Patterns of a Rectangular Block," Reports of Research Institute for Applied Mechanics, Kyushu University, Japan, Vol. XIX, No. 65, March 1972.

[2] Ericsson, L.E. and Reding, J.P., "Analysis of Flow Separation Effects on the Dynamics of a Large Space Booster," *Journal of Spacecraft and Rockets,* Vol. 2, July-Aug. 1965, pp. 481-490.

[3] Ericsson, L.E., "Aeroelastic Instability Caused by Slender Payloads," *Journal of Spacecraft and Rockets,* Vol. 4, Jan. 1967, pp. 65-73.

[4] Ericsson, L.E. and Reding, J.P., "Dynamics of Separated Flow Over Blunt Bodies," NASA CR-76912, Dec. 1965.

[5] Reding, J.P. and Ericsson, L.E., "Aeroelastic Stability of the 747/Orbiter," *Journal of Aircraft,* Vol. 14, Oct. 1977, pp. 988-993.

[6] Reding, J.P. and Ericsson, L.E., "Effects of Flow Separation on Shuttle Longitudinal Dynamics and Aeroelastic Stability," *Journal of Spacecraft and Rockets,* Vol. 14, Dec. 1977, pp. 711-718.

[7] Ericsson, L.E. and Reding, J.P., "Aeroelastic Analysis of the Space Shuttle External Tank Cable Trays, Final Technical Report," Lockheed Missiles and Space Company, Inc., Sunnyvale, Calif., LMSC D766543, April 1981.

[8] Parkinson, G.V., "Aeroelastic Galloping in One Degree of Freedom," *Proceedings of the Conference on Wind Effects on Buildings and Structures Held at NPL, England, in June, 1963,* Vol. II, Her Majesty's Stationery Office, London, 1965, pp. 582-609.

[9] Nakamura, Y. and Tomonari, Y., "Pressure Distributions on Rectangular Prisms at Small Incidence," *Transactions of the Japan Society for Aeronautical and Space Sciences,* Vol. 21, No. 54, 1979, pp. 205-213.

[10] LaBerge, J.G., "Effect of Flare on the Dynamic and Static Moment Characteristics of a Hemisphere-Cylinder Oscillating in Pitch at Mach Numbers from 0.3 to 2.0," National Research Council of Canada, Aeronautical Report LR-295, Jan. 1981.

[11] Ericsson, L.E., "Separated Flow Effects on the Static and Dynamic Stability of Blunt Nosed Cylinder Flare Bodies," NASA CR 76919, Dec. 1965.

[12] Ericsson, L.E. and Reding, J.P., "Dynamic Stall Analysis in Light of Recent Numerical and Experimental Results," *Journal of Aircraft,* Vol. 13, April 1976, pp. 248-255.

[13] Ericsson, L.E. and Reding, J.P., "Dynamic Stall at High Frequency and Large Amplitudes," *Journal of Aircraft,* Vol. 17, March 1980, pp. 136-142.

[14] Ericsson, L.E. and Reding, J.P., "Stall Flutter Analysis," *Journal of Aircraft,* Vol. 10, Jan. 1973, pp. 5-13.

[15] Ericsson, L.E. and Reding, J.P., "Unsteady Airfoil Stall, Review and Extension," *Journal of Aircraft,* Vol. 8, Aug. 1971, pp. 609-616.

[16] Ericsson, L.E. and Reding, J.P., "Aeroelastic Stability of Space Shuttle Protuberances," AIAA Paper 81-1672, Aug. 1981.

[17] *Aviation Week,* Jan. 5, 1981, p. 51.

[18] *Time,* Jan. 12, 1981, front page.

[19] LaBerge, J.G., "Dynamic Wind Tunnel Tests of the Shuttle External Tank Cable Trays at Subsonic Speeds," National Research Council of Canada, LTR-UA-55, Feb. 1981.